Journal of Power Sources 196 (2011) 6622–6628

Contents lists available at ScienceDirect

Journal of Power Sources

journal homepage: www.elsevier.com/locate/jpowsour

Novel zinc porphyrin with phenylenevinylene *meso*-substituents: Synthesis and application in dye-sensitized solar cells

J.A. Mikroyannidis[a,*], G. Charalambidis[b], A.G. Coutsolelos[b,*], P. Balraju[c], G.D. Sharma[c,d,**]

[a] Chemical Technology Laboratory, Department of Chemistry, University of Patras, GR-26500 Patras, Greece
[b] Department of Chemistry, University of Crete, Laboratory of Bioinorganic Chemistry, Voutes Campus, P.O. Box 2208, 71003 Heraklion, Crete, Greece
[c] Physics Department, Molecular Electronic and Optoelectronic Device Laboratory, JNV University, Jodhpur (Raj.) 342005, India
[d] R & D centre for Engineering and Science, Jaipur Engineering College, Kukas, Jaipur (Raj.), India

ARTICLE INFO

Article history:
Received 3 January 2011
Received in revised form 9 March 2011
Accepted 12 March 2011
Available online 22 March 2011

Keywords:
Zinc porphyrin
Dye-sensitized solar cells
Phenylnevinylene
Cyanovinylene
Photosensitizer

ABSTRACT

A novel zinc porphyrin, **P**, with phenylenevinylene segments at two opposite *meso*-positions and carboxyphenyl at the other two *meso*-positions of the porphyrin ring, was synthesized and characterized. The phenylenevinylene substituents were terminated with electron-accepting 4-nitro-α-cyanostilbene units. Elongation of the π-conjugation enhanced the solubility of **P** as well as broadened and strengthened the absorption spectrum. We have investigated the application of **P** in quasi solid state dye-sensitized solar cells (DSSCs). Under illumination intensity of 100 mW cm^{-2}, a power conversion efficiency of 2.90% was obtained for the DSSC based on **P** as sensitizer, which was significantly improved to 4.22% upon addition of deoxycholic acid (DCA) into the **P** solution for TiO_2 sensitization. Coadsorption of DCA decreased the dye adsorption, but significantly improved both short circuit current (J_{sc}) and open circuit voltage (V_{oc}). The breakup of π stacked aggregates might improve the electron injection yield and thus J_{sc}. The electrochemical impedance data indicate that the electron lifetime was improved by the coadsorption of DCA, which was attributed to the improvement in both V_{oc} and J_{sc}. The increase in J_{sc} has also been attributed to the reduction of the back reaction i.e., the recombination of electrons with tri-iodide ions.

1. Introduction

Dye-sensitized solar cells (DSSCs) were developed by Grätzel and co-workers in the early 1990s [1] as an alternative to solid-state cells. Since that time, a considerable amount of work has been carried out in an effort to improve the efficiency of such cells. The most efficient dyes to date are based on ruthenium polypyridyl systems, where efficiencies of up to 11% have been obtained [2]. In recent years, the interest in organic dyes as substitutes for noble metal complexes has increased in terms of economic dye production as well as for feasible control of the factors which influence the efficiency of cells [3]. Among the organic dyes, porphyrins and their derivatives have been regarded as potential photosensitizers in DSSCs because they possess an intense Soret band at 400–450 nm and moderate Q bands at 500–650 nm. Moreover, they contain a conveniently modifiable macrocyclic structure and ultrafast electron injection properties together with slow charge recombination kinetics comparable to those of Ru dyes [4]. However, porphyrin dyes showed low efficiency compared with Ru dyes for DSSCs due to a poor match with the solar light distribution. To improve the performance of porphyrin dyes, porphyrins with extended π-conjugation and efficient anchoring groups have been designed and this led to better photovoltaic performance [5]. Adsorbing porphyrins with modified structures onto TiO_2 nanocrystalline films thus provides an opportunity to improve DSSC applications. The best performance of porphyrin-sensitized solar cells based on liquid electrolyte has attained efficiency of 7.1% [6]. A recently reported series of porphyrin dyes with donor–acceptor (D–A) substituents exhibit promising photovoltaic properties [7]. Very recently, Grätzel et al. reported the achievement of an 11% solar-to-electric power conversion efficiency under standard (AM 1.5G, 100 mW cm^{-2} intensity) reporting conditions by using a judiciously tailored porphyrin dye, YD-2 [8]. On the other hand, a conjugated copolymer of poly(phenylenevinylene) containing metalloporphyrin incorporated into the polymer backbone has been synthesized [9]. Moreover, a multidomain compound with applications in the area of organic solar cells (OSCs) which contains zinc porphyrin and oligo phenylenevinylene moieties has been synthesized [10].

Several factors are considered important when seeking or designing an efficient photosensitizer. The appropriate sensitizers should have these properties: the ability to adsorb strongly

* Corresponding authors. Tel.: +30 2610 997115; fax: +30 2610 997118.
** Corresponding author at: Physics Department, Molecular Electronic and Optoelectronic Device Laboratory, JNV University, Jodhpur (Raj.) 342005, India. Tel.: +91 0291 2720857; fax: +91 0291 2720856.
E-mail addresses: mikroyan@chemistry.upatras.gr, mikroyan@googlemail.com (J.A. Mikroyannidis), coutsole@chemistry.uoc.gr (A.G. Coutsolelos), sharmagd_in@yahoo.com (G.D. Sharma).

0378-7753/$ – see front matter © 2011 Elsevier B.V. All rights reserved.
doi:10.1016/j.jpowsour.2011.03.023

on the surface of a semiconductor, absorption of light in the visible and NIR region for efficient light harvesting, an excited-state reduction potential negative enough for efficient electron injection, a ground-state reduction potential positive enough for efficient regeneration of the dye, and a small reorganizational energy for efficient excited- and ground-state electrochemical processes [11]. The relation between the orientation of attached porphyrins with respect to TiO_2 nanocrystalline surfaces and the cell performance has been investigated [12,13]. For porphyrins [6,12,14], an efficient injection of electrons from the photosensitizer into a semiconductor is considered a crucial factor in developing an efficient DSSC. Apart from the effect of cosensitization [15], the performance of a cell can be improved through appropriate modification of a dye structure with a selected link.

Herein, we designed and synthesized a new zinc porphyrin **P** with broad absorption which was used as photosensitizer for DSSCs. The central porphyrin of **P** acts as electron-donor and the two terminal 4-nitro-α-cyanostilbenes act as electron-acceptors. The two carboxyphenyls act as anchoring groups. The long phenylenevinyle substituents at the two opposite *meso* positions of porphyrin reduce the aggregation between neighbouring porphyrins on the TiO_2 surface by sterically hindering the porphyrin core. These phenylenevinylene π-conjugated segments are expected to broaden the absorption of **P** and enhance the solubility. We report the photovoltaic properties of **P** sensitized quasi solid state DSSCs and the effect of deoxycholic acid (DCA) coadsorption on the solar cell performance. The power conversion efficiency (PCE) was increased from 2.90% to 4.22% upon sensitizing the TiO_2 film with the **P** solution containing 40 mM of DCA. The increase in the PCE has been related to the improved electron injection efficiency and higher electron lifetime.

2. Experimental

2.1. Reagents and solvents

4-Vinylbenzaldehyde was synthesized from the reaction of 4-bromobenzaldehyde with tributyl(vinyl)stannane in toluene in the presence of $Pd(PPh_3)_4$ [16]. 4-Nitrobenzylcyanide was synthesized from the nitration of benzyl cyanide with concentrated nitric and sulfuric acid [17]. It was recrystallized from ethanol. Dipyrromethane was prepared according to the literature procedure [18]. *N,N*-dimethylformamide (DMF) and tetrahydrofuran (THF) were dried by distillation over CaH_2. All other reagents and solvents were commercially purchased and were used as supplied.

2.2. Preparation of compounds

2.2.1. Compound *1*

A solution of 4-carboxymethylbenzaldehyde (0.45 g, 2.7 mmol) and dipyrromethane (0.4 g, 2.7 mmol) in 300 mL of dichloromethane was purged with nitrogen for 30 min. The flask was shielded from light with aluminium foil, trifluoroacetic acid (0.13 mL, 1.7 mmol) was added and the solution stirred at room temperature for 3.5 h. 2,3-Dichloro-5,6-dicyano-1,4-benzoquinone (DDQ, 0.85 g, 3.7 mmol) was added and the solution stirred for a further 1.5 h. The mixture was neutralized with triethylamine (1.5 mL) and poured directly onto a silica gel pad packed in dichloromethane. The product eluted with 99.5:0.5 CH_2Cl_2:Et_3N. On removal of the solvent porphyrin **1** was obtained as a purple solid (360 mg, 46%) and was used without any other purification. Compound **1** is not soluble enough to obtain NMR spectrum.

FT-IR (KBr, cm^{-1}): 2954 (C–H stretching of methyl); 1720 (carbonyl stretching of carboxymethyl); 1286 (C–O–C stretching of carboxymethyl).

HRMS Calcd for $C_{36}H_{27}N_4O_4$ $(M+H)^+$ 579.2032. Found, 579.2041.

UV–vis λabs ($CHCl_3$) (ε, $mM^{-1}\,cm^{-1}$): 409 (388.5), 503 (17.1), 538 (7.3), 589 (5.7), 630 (2.2).

2.2.2. Compound *2*

To a stirred solution of porphyrin **1** (70 mg, 0.12 mmol) in dichloromethane (35 mL) a solution of zinc acetate dihydrate (0.13 g, 0.6 mmol) in methanol (10 mL) was added. The reaction was stirred for 16 h at room temperature. Evaporation of the solvent and flash chromatography on silica, eluting with 98:2 CH_2Cl_2:EtOH, was carried out to remove excess zinc salts. Evaporation of the solvent gave the zinc porphyrin **2** as a purple solid (75 mg, 97%).

FT-IR (KBr, cm^{-1}): 2946 (C–H stretching of methyl); 1719 (carbonyl stretching of carboxymethyl); 1280 (C–O–C stretching of carboxymethyl).

^{1}H NMR (500 MHz, $CDCl_3$/1% pyridine–d_5) ppm: 10.21 (s, 2H, methynic); 9.35 (d, J = 4.5 Hz, 4H, β-pyrrole); 8.98 (d, J = 4.0 Hz, 4H, β-pyrrole); 8.42 (d, J = 8.0 Hz, 4H, phenylene ortho to carboxymethyl); 8.30 (d, J = 8.0 Hz, 4H, phenylene meta to carboxymethyl); 4.09 (s, 6H, carboxymethyl).

^{13}C NMR (75 MHz, $CDCl_3$/1% pyridine–d_5) ppm: 167.6, 149.6, 149.5, 148.3, 134.9, 131.9, 129.0, 127.7, 118.3, 106.2, 52.4.

HRMS Calcd for $C_{36}H_{25}N_4O_4Zn$ $(M+H)^+$ 641.1167. Found, 641.1175.

UV–vis λabs ($CHCl_3$) (ε, $mM^{-1}\,cm^{-1}$): 409 (404.7), 537 (16.6), 570 (3.7).

2.2.3. Compound *3*

Zinc porphyrin **2** (50 mg, 0.078 mmol) was dissolved in chloroform (25 mL) with pyridine (35 μL). The solution was cooled to 0 °C and *N*-bromosuccinimide (NBS, 30 mg, 0.17 mmol) was added. The resulting green mixture was stirred for 25 min and then quenched with acetone (7 mL). The solvents were removed under reduced pressure and the residue was purified by column chromatography on silica. The desired porphyrin **3** eluted with dichloromethane to give a purple solid (60 mg, 96%).

FT-IR (KBr, cm^{-1}): 2945 (C–H stretching of methyl); 1720 (carbonyl stretching of carboxymethyl); 1278 (C–O–C stretching of carboxymethyl).

^{1}H NMR (500 MHz, $CDCl_3$/1% pyridine–d_5) ppm: 9.64 (d, J = 5.0 Hz, 4H, β-pyrrole); 8.78 (d, J = 4.5 Hz, 4H, β-pyrrole); 8.41 (d, J = 8.0 Hz, 4H, phenylene ortho to carboxymethyl); 8.20 (d, J = 8.0 Hz, 4H, phenylene meta to carboxymethyl); 4.10 (s, 6H, carboxymethyl).

^{13}C NMR (75 MHz, $CDCl_3$/1% pyridine–d_5) ppm: 167.4, 150.4, 150.3, 147.6, 134.7, 133.4, 133.0, 129.5, 127.7, 120.7, 105.2, 52.5.

HRMS Calcd for $C_{36}H_{23}Br_2N_4O_4Zn$ $(M+H)^+$ 796.9378. Found, 796.9371.

UV–vis λabs ($CHCl_3$) (ε, $mM^{-1}\,cm^{-1}$): 426 (391.7), 555 (19.7), 592 (5.2).

2.2.4. Compound *4*

A flask was charged with a mixture of **3** (95 mg, 0.119 mmol), 4-vinylbenzaldehyde (31.4 mg, 0.238 mmol), $Pd(OAc)_2$ (1.1 mg, 0.005 mmol), P(*o*-tolyl)$_3$ (8.3 mg, 0.027 mmol), DMF (5 mL) and triethylamine (3 mL). The flask was degassed and purged with N_2. The mixture was heated at 90 °C for 18 h under N_2. Then, it was filtered and the filtrate was poured into methanol. The precipitate was isolated by centrifugation and washed with methanol. The crude product was purified by dissolution in THF and precipitation into methanol (67.5 mg, 63%).

FT-IR (KBr, cm^{-1}): 2976 (C–H stretching of methyl); 1720 (carbonyl stretching of carboxymethyl); 1703 (carbonyl stretching of formyl); 1278 (C–O–C stretching of carboxymethyl).

^{1}H NMR ($CDCl_3$) ppm: 9.95 (s, 2H, formyl); 8.83 (m, 8H, β-pyrrole); 7.92 (m, 4H, phenylene ortho to carboxymethyl); 7.76

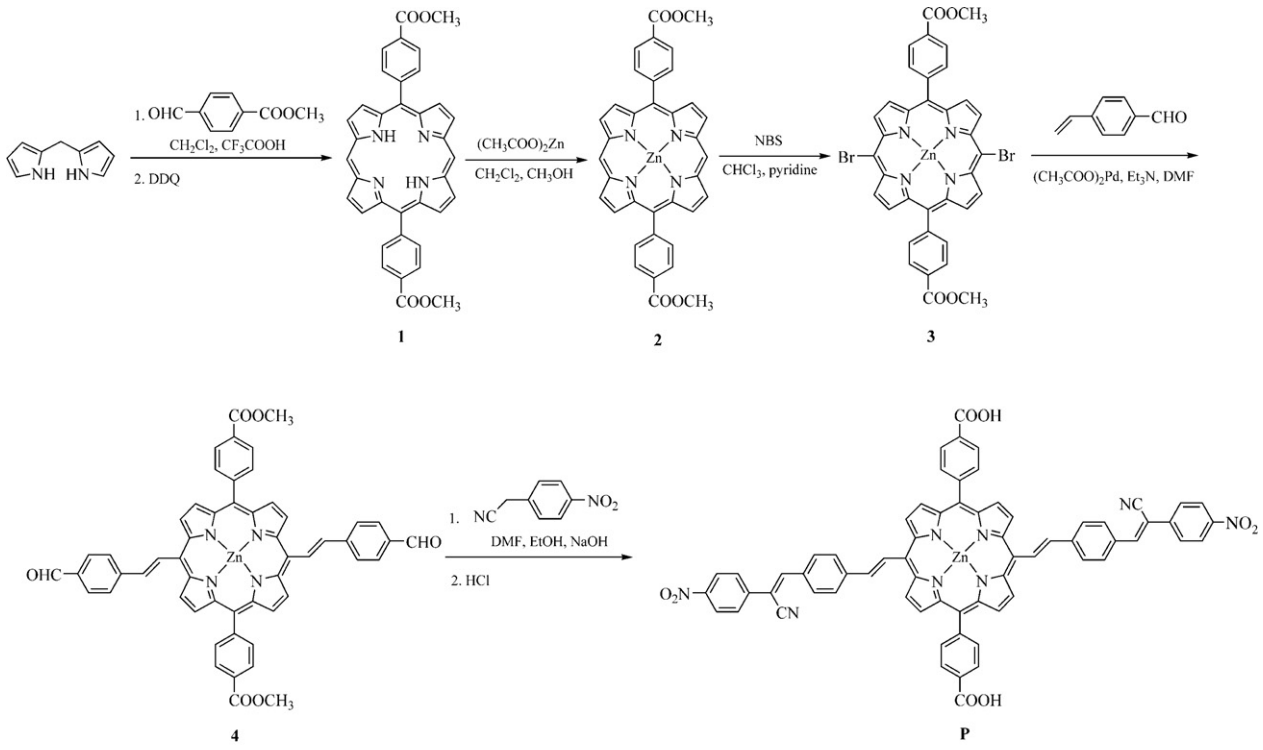

Scheme 1. Synthesis of **P**.

(m, 4H, phenylene ortho to formyl); 7.32-7.23 (m, 8H, other phenylene); 7.21 (m, 4H, vinylene); 3.88 (s, 6H, carboxymethyl).

HRMS Calcd for $C_{54}H_{36}N_4O_6Zn$ $(M)^+$ 900.1926. Found, 900.1921.

UV–vis λabs (THF) (ε, $mM^{-1}\,cm^{-1}$): 427 (385.2), 559 (18.1), 606 (4.9).

2.2.5. Compound *P*

A flask was charged with a solution of **4** (0.1071 g, 0.119 mmol) and 4-nitrobenzylcyanide (38.5 mg, 0.238 mmol) in DMF (15 mL). Sodium hydroxide (0.20 g, 5.0 mmol) dissolved in ethanol (5 mL) was added portionwise to the stirred solution. The mixture was stirred and heated at 80 °C for 3 h under N_2. Then, dilute hydrochloric acid was added to the solution and **P** precipitated as a dark green solid. The crude product was purified by dissolution in THF and precipitation into methanol (77.2 mg, 56%).

FT-IR (KBr, cm^{-1}): 3350 (O–H stretching of carboxyl); 1710 (carbonyl stretching of carboxyl); 2213 (cyano); 1528, 1346 (nitro); 962 (trans vinylene bond).

^{1}H NMR ($CDCl_3$) ppm: 12.09 (br, 2H, carboxyl); 8.83 (m, 8H, β-pyrrole); 8.19-8.12 (m, 8H, phenylene ortho to nitro and ortho to carboxyl); 7.84 (s, 2H, cyanovinylene); 7.68-7.30 (m, 16H, other phenylene); 7.21 (m, 4H, vinylene).

HRMS Calcd for $C_{68}H_{40}N_8O_8Zn$ $(M)^+$ 1160.2261. Found, 1160.2269.

UV–vis λabs (THF) (ε, $mM^{-1}\,cm^{-1}$): 427 (384.1), 559 (20.7), 606 (5.3).

2.3. Characterization methods

^{1}H NMR spectra were recorded unless otherwise specified, as deuteriochloroform solutions using the solvent peak as internal standard on a Bruker AMX-500 MHz and Bruker DPX-300MHz spectrometers. IR spectra were recorded on a Perkin-Elmer 16PC FT-IR spectrometer with KBr pellets. UV–visible spectra were recorded on a Shimadzu UV-1700 PharmaSpec instrument. High resolution mass spectra were performed on a Bruker ultrafleXtreme MALDI-TOF/TOF spectrometer. Chromatography refers to flash chromatography and was carried out on SiO_2 (silica gel 60, SDS, 70-230 mesh ASTM).

The electrochemical properties of **P** were studied using cyclic voltammetry (CV). The **P** was coated on platinum disk and immersed in 0.1 M Bu_4NPF_6 acetonitrile solution. CV was recorded using platinum disk as working electrode and Ag/Ag+ as the reference electrode at the scan rate of 100 mV s^{-1}.

2.4. Fabrication of DSSCs and methods for their evaluation

The TiO_2 paste was prepared by mixing 1 g of TiO_2 powder (P25 Degussa), 0.2 mL of acetic acid and 0.1 mL of deionized water. Then, 60 mL of ethanol was slowly added while sonicating the mixture for 3 h. Finally, Triton X-100 was added and a well dispersed colloidal paste was obtained (TiO_2). The mixture was stirred vigorously for 2–4 h at room temperature and then stirred for 4 h at 80 °C to form a transparent colloidal paste. The TiO_2 paste was deposited on the F-doped tin oxide (FTO) coated glass substrates by the doctor blade technique. The TiO_2 films were sintered at 450 °C for 30 min. The sintered TiO_2 coated FTO films were soaked in a 0.2 M aqueous $TiCl_4$ for overnight in a closed chamber. After being washed with deionized water and fully rinsed with ethanol, the films were heated at 450 °C for 30 min, followed by cooling to 50 °C. The **P** was dissolved in THF solution (0.5 mM) and the prepared TiO_2 deposited FTO electrode was immersed in the sensitizer solution for 12 h and after sensitization the dye electrode was washed. The quasi solid state polymer electrolyte containing 0.0383 g of P25 TiO_2 powder, 0.1 g of LiI, 0.019 g of I_2, 0.264 g of PEO, and 44 μL of 4-*tert*-butyl pyridine in 1:1 acetone/propylene carbonate was prepared. The mixture was continuously stirred at 80 °C in water bath for about 4 h. The above prepared quasi solid state polymer gel electrolyte was spread on

the **P** sensitized TiO_2 film by spin coating to form the hole conducting layer. The counter electrode was platinized by spin coating H_2PtCl_4 solution (2 mg in 1 mL of isoproponol) onto the FTO coated glass substrate and then heated at 450 °C for 30 min in air. The dye sensitized photoelectrode containing the quasi solid state polymer electrolyte and the counter electrode were clamped together and separated by a 20 μm spacer.

The current–voltage characteristics (J–V) of the devices in dark and under illumination were measured by a semiconductor parameter analyser (Keithley 4200–SCS). A xenon light source (Oriel, USA) was used to give an irradiance of 100 mW cm^{-2} (equivalent of one sun at AM 1.5) at the surface of the device. The photoaction spectra of the devices was measured using a monochromator (Spex 500M, USA) and the resultant photocurrent was measured with Keithley electrometer (model 6514) which is interfaced to the computer by LABVIEW software. The electrochemical impedance spectra (EIS) measurements were carried out by applying bias equivalent to the V_{oc} of the device and recorded over a frequency of 1 mHz–10^5 Hz with an ac amplitude of 10 mV. The above measurements were recorded with an electrochemical impedance analyser equipped with FRA.

3. Results and discussion

3.1. Synthesis and characterization

Scheme 1 outlines the synthesis of **P**. Particularly, the 5,15-diaryl porphyrin **1** was readily prepared in one step by acid-catalyzed condensation of dipyrromethane with 4-carboxymethylbenzaldehyde, followed by *in situ* oxidation with DDQ. Metallation with zinc acetate furnished the desired zinc porphyrin **2** in good yield. Dibromoporphyrin **3** was prepared by reaction with two equivalents of NBS in the presence of pyridine. The Heck coupling of **3** with 4-vinylbenzaldehyde in DMF in the presence of triethylamine and palladium acetate afforded dialdehyde **4**. Finally, the condensation of **4** with 4-nitrobenzylcyanide in the presence of sodium hydroxide followed by hydrolysis of the ester and acidification with hydrochloric acid gave the target porphyrin **P**.

P was soluble in common organic solvents such as chloroform, dichloromethane and THF. It showed higher solubility than the intermediate compounds **1**–**4** owing to the increase in the organic moieties. It was characterized by FT-IR and ^1H NMR spectroscopy. The IR spectrum of **P** displayed characteristic absorption bands at 3350 (O–H stretching of carboxyl); 1710 (carbonyl stretching of carboxyl); 2213 (cyano); 1528, 1346 (nitro) and 962 cm^{-1} (trans vinylene bond). The ^1H NMR spectrum showed upfield signals at 12.09 (carboxyl), 8.83 (β-pyrrole) and 8.19-8.12 ppm (phenylene ortho to nitro and ortho to carboxyl). The cyanovinylene resonated at higher shift (7.84 ppm) than the vinylene (7.21 ppm) due to the presence of the electron-withdrawing cyano groups in the former.

3.2. Photophysical properties

Fig. 1a presents the UV–visible absorption spectra of **P** in both dilute (10^{-5} M) THF solution and thin film. They were very similar and showed a Soret band at 427 nm and Q-bands at 559 and 606 nm which are typical absorption peaks of zinc porphyrins. For comparison, Fig. 1b depicts the UV–visible absorption spectra in THF solution of **P** and intermediate compound **3**. It can be seen from this figure, that **P** showed broader and stronger absorption than **3** in the range of 300–750 nm. Broadening the absorption may remedy the weakness of porphyrins, resulting in improved photovoltaic (PV) performance. The broadening and strengthening of the absorption of **P** as compared to that of **3** is attributed to the extended conjugation of the π-systems in the *meso*-positions

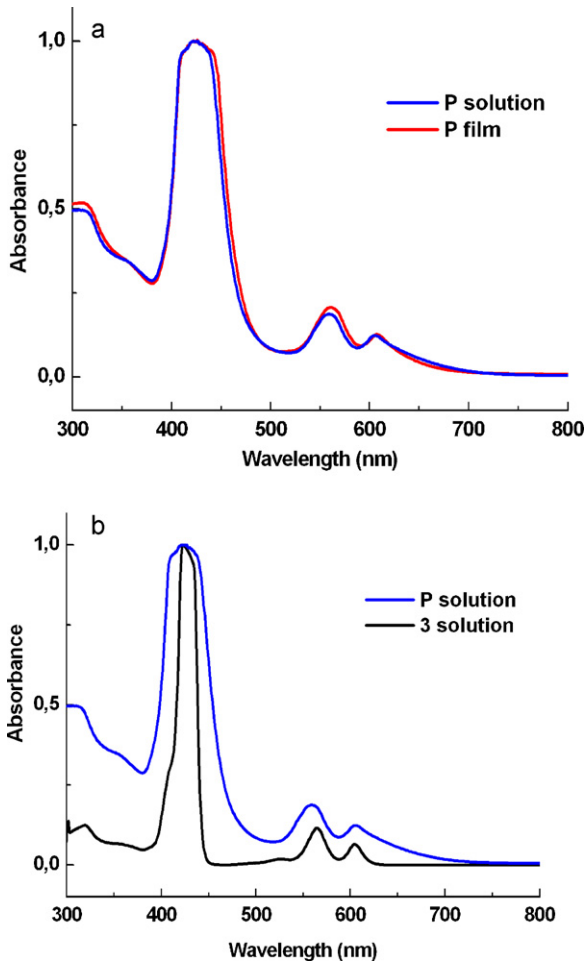

Fig. 1. UV–vis absorption spectra of **P** in THF solution and thin film (a) as well as of **P** and **3** in THF solution (b). The spectra were normalized with respect the Soret band.

of porphyrin. An intramolecular charge transfer (ICT) takes place between the electron-donating central porphyrin core and the electron-withdrawing terminal cyanovinylene 4-nitrophenyls. The extended conjugated moieties, which were inserted at the two opposite *meso*-positions of the porphyrin ring of **P** not only improved the absorption but also enhanced the solubility. Specifically, compound **3** was very slightly soluble in THF, so that thin films could not be obtained from solution. In contrast, **P** was readily soluble in THF and other common organic solvents thus allowing the preparation of films by the spin coating method and improving the processability.

Fig. 2 shows the UV–visible absorption spectrum of **P** adsorbed on the TiO_2 film. Comparison of this spectrum to the solution spectrum of **P** reveals that the Q-band in the absorption spectra of **P**/TiO_2 film is slightly red shifted and considerably broadened. The B band (Soret) band is also broadened. The broadened absorption bands (Q- and Soret) of the **P** adsorbed TiO_2 film may be due to intermolecular interactions of the molecules aggregated on the TiO_2 surface [19]. The blue shift in the Soret band is related to the H-type aggregation of **P** on the TiO_2 surface [20]. Moreover, the broadened absorption bands observed in the **P** adsorbed TiO_2 film spectra minimize the gap between the Soret and Q bands, resulting in increased spectral responses of the solar cells. Fig. 2 also compares the UV–visible spectra of **P** loaded TiO_2 films before and after DCA coadsorption. When DCA was included in the **P** solution, the **P** sensitized TiO_2 film cografted with DCA showed similar absorption peaks but the intensity of the absorption decreased, suggesting the amount of **P**

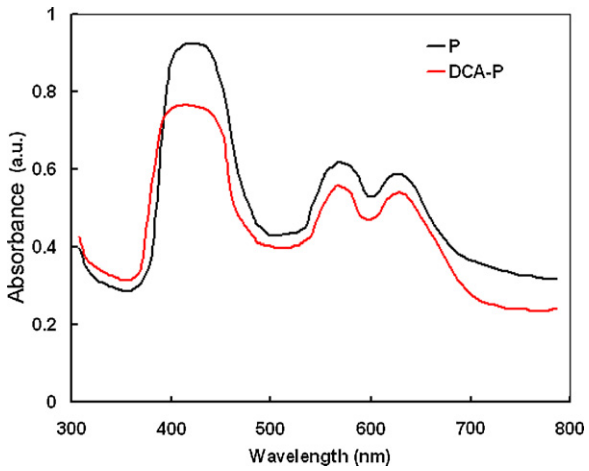

Fig. 2. Absorption spectra of **P** and DCA coadsorbed **P** sensitized TiO_2 films.

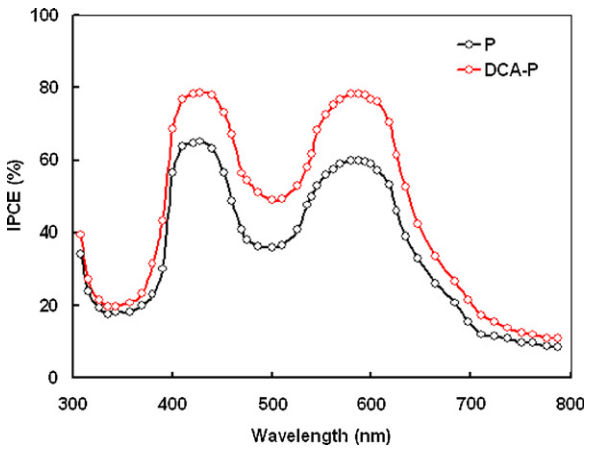

Fig. 3. IPCE spectra of the DSSCs based with and without DCA coadsorbant **P**.

on the TiO_2 surface has decreased. The competition of DCA with the **P** for binding to the TiO_2 surface is responsible for the decrease in the **P** adsorption (dye loading).

3.3. Electrochemical properties

To ensure efficient electron injection from the LUMO of the sensitizer into the conduction band of TiO_2, the LUMO level must be higher than the conduction band edge of TiO_2. The HOMO level of the sensitizer must be lower than the redox potential of I^-/I_3^- couple for efficient regeneration of the sensitizer cation after the photoinduced electron injection into the conduction band of TiO_2. The HOMO (E_{HOMO}) and LUMO (E_{LUMO}) energy levels of **P** were estimated from the oxidation onset (0.80 V) and reduction onset (−1.15 V) potentials, observed in cyclic voltammograms according to following expression [21].

$$E_{HOMO} = -(E_{ox} + 4.7)\,eV$$

$$E_{LUMO} = -(E_{red} + 4.7)\,eV$$

where E_{ox} and E_{red} are the oxidation and reduction onset potentials, respectively, measured with reference the Ag/Ag+ redox potential (4.7 V). The difference between the LUMO energy level of sensitizer and the conduction band edge of TiO_2 should be higher than 0.2 eV for efficient electron injection [22]. The LUMO and HOMO energy levels for **P** are −3.55 eV and −5.50 eV, respectively. This indicates that the LUMO level of **P** is sufficiently higher than the conduction band of TiO_2 (−4.0 eV) and consequently an efficient electron transfer from the LUMO of **P** into the conduction band of TiO_2 is possible. Moreover, the HOMO energy level of **P** is lower than the standard potential of I^-/I_3^- redox couple (−4.85 eV vs vacuum). This indicates that sufficient driving force exists for the regeneration of the oxidised **P** in DSSCs.

3.4. Photovoltaic performance

The incident photons to current efficiency (IPCE) spectra of the devices are shown in Fig. 3 The IPCE spectra of the device are similar to the corresponding absorption spectra of **P** sensitized TiO_2 electrode, indicating that all the photons absorbed by **P** are contributing to the photocurrent. Fig. 3 also compares the IPCE spectra of the DSSCs based on TiO_2 photoanode sensitized with **P** alone and with both **P** - DCA (40 mM). The maximum IPCE value is about 65% and 60% in the Soret and Q band, respectively for **P** sensitized DSSCs. Upon addition of the DCA in the **P** solution, the IPCE in both bands was enhanced significantly. The IPCE is the product of the electron injection efficiency, light harvesting efficiency and charge collection efficiency. It can be seen from the absorption spectra of **P** sensitized TiO_2 film that the light harvesting efficiency is higher than that for DCA added **P** sensitized TiO_2 film. Therefore, the higher value of IPCE for the DSSC based on DCA added **P** sensitized DSSCs may be due to the increase in the electron injection efficiency and the charge collection efficiency. The lower charge collection efficiency or lower IPCE is attributed to the charge recombination caused by the dye aggregation or close π–π^* stacking. Upon coadsorption with DCA, although the amount of dye on the TiO_2 surface is reduced, the IPCE spectra of the DSSCs based on this become broader as compared to the IPCE spectra of DSSC based on **P**. Therefore, the improvement in the IPCE is directly attributed to the reduction of the dye adsorption. We can conclude that the coadsorption is necessary to break up the dye aggregates, which is essential for IPCE improvement. Upon coadsorption of DCA, this acts as spacer among the dye molecules and thus suppresses the π–π interaction of the dye molecules that retards charge recombination and hence improves the IPCE [23].

The J–V characteristics of the DSSCs with or without DCA are shown in Fig. 4a and the PV parameters i.e., short circuit current (J_{sc}), open circuit voltage (V_{oc}), fill factor (FF) and power conversion efficiency (PCE) are summarized in Table 1 The above PV results indicate that the coadsorption of DCA is an effective approach to improve the DSSC performance. All the PV parameters have been improved upon the DCA adsorption. The increase in V_{oc} has been attributed to the fact that the adsorption of DCA charges the surface of TiO_2 negatively and shifts the conduction band edge negatively [24]. The increase in the V_{oc} also indicates that the charge recombination was suppressed by DCA. To understand the role of DCA in improving the PV performance of the DSSC, the effect of the DCA on dark current was studied as shown in Fig. 4b. It is found that the dark current onset voltage shifted to a larger value, and the dark current was also reduced upon the coadsorption of DCA. This reduction in dark current indicates that coadsorption of DCA leads to suppression of the charge recombination between the injected electrons and the I_3^- ions in the electrolyte, thus increasing both

Table 1
Photovoltaic parameters of quasi solid state DSSCs based on **P** and DCA–**P** sensitizer.

Sensitizer	J_{sc} (mA cm^{-2})	V_{oc} (V)	FF	PCE (%)
P	8.8	0.70	0.47	2.90
DCA (40 mM)-**P**	10.3	0.76	0.54	4.22

J_{sc}, short circuit current; V_{oc}, open circuit voltage; FF, fill factor; PCE, power conversion efficiency.

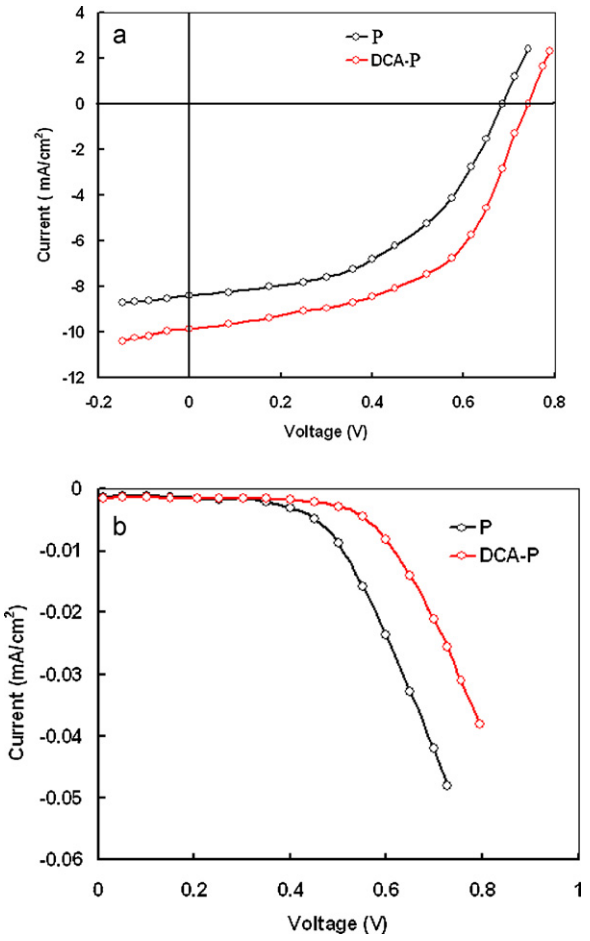

Fig. 4. Current–voltage characteristics for DSSCs sensitized with and without DCA coadsorbant sensitized (a) under illumination, (b) in dark.

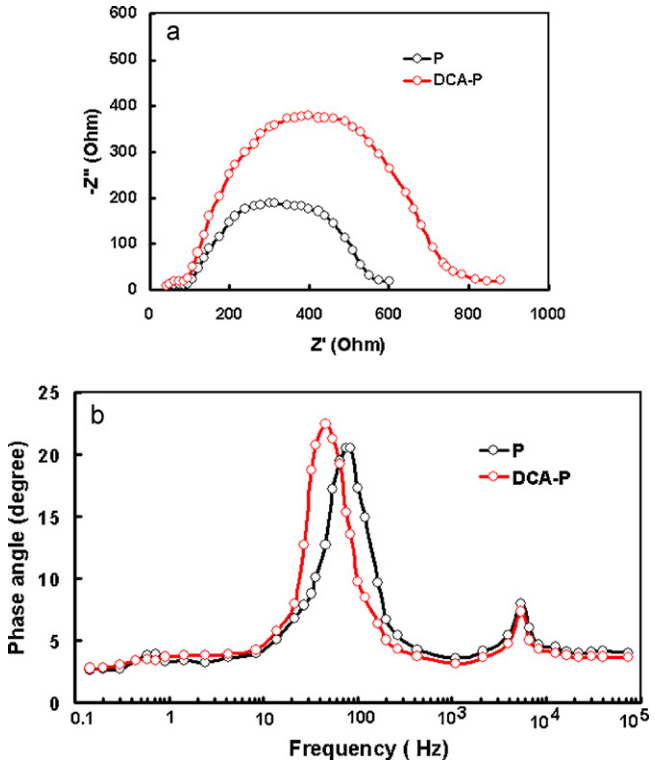

Fig. 5. Electrochemical impedance spectra (a) Nyquist plots, (b) Bode plots, of the DSSCs based on **P** and DCA–**P**, in dark.

V_{oc} and J_{sc}. The enhancement of V_{oc} is usually related to the negative shift of conduction band or suppression of charge recombination. The breakup of π-stacked aggregates might improve the electron injection efficiency and thus the J_{sc} [25].

Electrochemical impedance spectroscopy is a powerful tool for identifying electronic and ionic transport processes in DSSCs, which provides valuable information for understanding the photovoltaic parameters [26]. The tendency of charge recombination at the TiO_2/electrolyte interface and the movement of TiO_2 conduction band edge were also examined by EIS measurements in dark with applied voltage equivalent of V_{oc} of the device. The Nyquist plots in dark are shown in Fig. 5a for the DSSCs based on **P** and DCA–**P**, measured under a forward bias equivalent to V_{oc} of the DSSCs. The equivalent circuit shown in Fig. 6 was used to fit the experimental data of the DSSCs. R_s, is the series resistance accounting for the transport resistance of the FTO and the electrolyte. C_μ and R_{ct} are the chemical capacitance and charge recombination resistance at the TiO_2/electrolyte interface, respectively. C_{pt} and R_{pt} are the interfacial capacitance and charge transport resistance at the Pt/electrolyte interface, respectively. For both DSSCs based on with and without DCA coadsorbant **P** sensitized TiO_2 electrodes, show three semicircles. The larger semicircle in the middle frequency region is clearly observed in both DSSCs, corresponding to the charge transfer at the TiO_2/electrolyte interface [27]. The charge transfer resistance (R_{ct}) fitted to DSSCs based on DCA coadsorbant **P** (745 Ω) is higher than that of **P** (432 Ω), indicating that recombination rate in the DSSC based on former is slower as compared to the latter. In addition, the chemical capacitance (C_μ) of the DSSC based on **P** (34.6 μF) is larger than that for DCA coadsorbant **P** (28.8 μF), suggesting that a negative shift in the conduction band edge (CB) of TiO_2 was induced by the DCA coadsorbant [28]. Both slow charge recombination process and negative shift in the CB of TiO_2 contribute to the higher V_{oc} of the DSSC based on DCA coadsorbant **P** sensitized TiO_2 electrode. The EIS bode plot (frequency range from 0.1 Hz to 10^5 Hz), shown in Fig. 5b, exhibits two frequency peaks for the electron transfer at the TiO_2/dye/electrolyte interface (middle frequency region, 10–100 Hz) and redox charge transfer at counter electrode (higher frequency region, beyond 1000 Hz) in increasing order of frequency [29]. The peak of the middle frequency region is related to the charge recombination rate and its reciprocal is regarded as electron lifetime [27,30]. The peak in the frequency region of 10–100 Hz, shifts to a smaller value for DCA coadsorbant **P** sensitized DSSC as compared to that for **P** sensitized DSSC, indicating an increase in the electron lifetime upon the DCA coadsorbant. The increase in the lifetime (16 ms and 25 ms for **P** and DCA–**P** sensitized, respectively) of the electron for the DSSC based on the DCA–**P** sensitizer indicates an improvement in both electron injection efficiency and charge collection efficiency leading to an enhancement of J_{sc}. The Bode plots in the lower frequency region do not show any distinguishable peak, but only an arc is observed below 3 Hz.

In order to gain more insight into the electron transport in DSSCs, the EIS i.e., Nyquist plot of the DSSCs was also measured

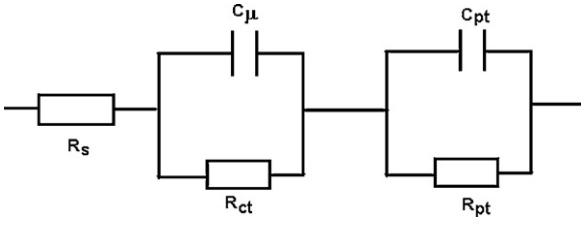

Fig. 6. Equivalent circuit used to fit the electrochemical impedance spectra.

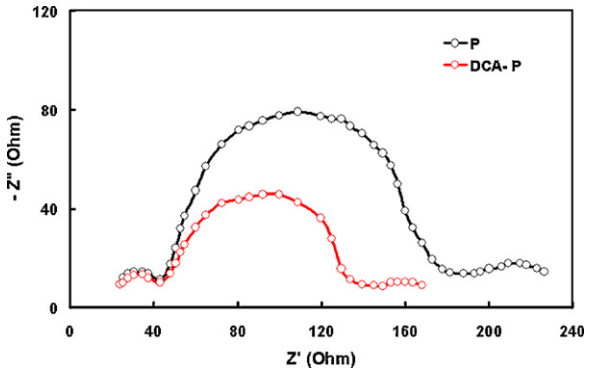

Fig. 7. Electrochemical impedance spectra i.e., Nyquist plots of DSSCs based on **P** and DCA–**P**, under illumination.

under illumination (100 mW cm^{-2}). As shown in Fig. 7, the radius of the semicircle in the middle frequency region is larger for the DSSC based on **P** than that for DCA–**P**. These results indicate that the charge transport in the DSSC based on DCA–**P** is faster than DCA–**P**, which coincides with the overall PCE of DSSCs [31].

4. Conclusions

A novel zinc porphyrin **P** was successfully synthesized by a five-step reaction sequence. It contained phenylenevinylene substituents at two opposite *meso*-positions of the porphyrin ring, which broadened the absorption spectrum and enhanced the solubility. The PV performance of **P** as sensitizer in nanocrystalline TiO_2 solar cells was investigated using polymer gel quasi solid state electrolyte and achieved a PCE of about 2.90%, which has been further improved up to 4.22%, upon addition of DCA to the **P** solution for TiO_2 sensitization. Coadsorption of DCA reduced the dye loading, but improved the J_{sc}, significantly (from 8.8 mA cm^{-2} to 10.3 mA cm^{-2}). The increase in the J_{sc} has been related to the improved electron injection efficiency and the charge collection efficiency. The improvement of V_{oc} is attributed to the suppressed charge recombination, which was revealed by the increase in electron lifetime.

References

[1] B. O'Regan, M. Grätzel, Nature 353 (1991) 737.
[2] M.K. Nazeeruddin, F. De Angelis, S. Fantacci, A. Selloni, G. Viscardi, P. Liska, S. Ito, B. Takeru, M. Grätzel, J. Am. Chem. Soc. 127 (2005) 16835.
[3] (a) D.P. Hagberg, T. Edvinsson, T. Marinado, G. Boschloo, A. Hagfeldt, L. Sun, Chem. Commun. (2006) 2245;
(b) Z. Ning, Q. Zhang, W. Wu, H. Pei, B. Liu, H. Tian, J. Org. Chem. 73 (2008) 3791;
(c) A. Burke, L. Schmidt-Mende, S. Ito, M. Grätzel, Chem. Commun. (2007) 234.
[4] (a) M. Tanaka, S. Hayashi, S. Eu, H. Imahori, Chem. Commun. (2007) 2069;
(b) Y. Tachibana, S.A. Haque, I.P. Mercer, J.R. Durrant, D.R. Klug, J. Phys. Chem. B 104 (2000) 1198.
[5] (a) Q. Wang, W.M. Campbell, E.E. Bonfantani, K.W. Jolley, D.L. Officer, P.J. Walsh, K. Gordon, R.H. Baker, M.K. Nazeeruddin, M. Grätzel, J. Phys. Chem. B 109 (2005) 15397;
(b) S. Hayashi, M. Tanaka, H. Hayashi, S. Eu, T.U. Meyama, Y. Matano, Y. Araki, H. Imahori, J. Phys. Chem. C 112 (2008) 15576;
(c) N. Koumura, Z.S. Wang, S. Mori, M. Miyashita, E. Suzuki, K. Hara, J. Am. Chem. Soc. 128 (2006) 14256;
(d) S. Eu, S. Hayashi, T. Umeyama, A. Oguro, M. Kawasaki, N. Kadota, Y. Matano, H. Imahori, J. Phys. Chem. C 111 (2007) 3528.
[6] W.M. Campbell, K.W. Jolley, P. Wagner, K. Wagner, P.J. Walsh, K.C. Gordon, L. Schmidt-Mende, M.K. Nazeeruddin, Q. Wang, M. Grätzel, D.L. Officer, J. Phys. Chem. C 111 (2007) 11760.
[7] (a) H.-P. Lu, C.-Y. Tsai, W.-N. Yen, C.-P. Hsieh, C.W. Lee, C.-Y. Yeh, E.W.G. Diau, J. Phys. Chem. C 113 (2009) 20990;
(b) C.-P. Hsieh, H.-P. Lu, C.-L. Chiu, C.-W. Lee, S.-H. Chuang, C.-L. Mai, W.-N. Yen, S.-J. Hsu, E.W.G. Diau, C.-Y. Yeh, J. Mater. Chem. 20 (2010) 1127.
[8] T. Bessho, S.M. Zakeeruddin, C.-Y. Yeh, E.W.G. Diau, M. Grätzel, Angew. Chem. 122 (2010) 1.
[9] (a) B. Jiang, W.E. Jones Jr., Macromolecules 30 (1997) 5575;
(b) F.C. Krebs, O. Hagemann, M. Jorgensen, Sol. Energy Mater. Sol. Cells 83 (2004) 211;
(c) F.C. Krebs, O. Hagemann, H. Spanggaard, J. Org. Chem. 68 (2003) 2463.
[10] O. Hagemann, M. Jørgensen, F.C. Krebs, J. Org. Chem. 71 (2006) 5546.
[11] F. Odobel, E. Blart, M. Lagree, M. Villieras, H. Boujtita, N.E. Murr, S. Caramori, C.A. Bignozzi, J. Mater. Chem. 13 (2003) 502.
[12] W.M. Campbell, A.K. Burrell, D.L. Officer, K.W. Jolley, Coord. Chem. Rev. 248 (2004) 1363.
[13] C.A. Bignozzi, R. Argazzi, C. Kleverlaan, J. Chem. Soc. Rev. 29 (2000) 87.
[14] M.K. Nazeeruddin, R. Humphry-Baker, D.L. Officer, W.M. Campbell, A.K. Burrell, M. Grätzel, Langmuir 20 (2004) 6514.
[15] J.-J. Cid, J.-H. Yum, S.-R. Jang, M.K. Nazeeruddin, E. Martínez-Ferrero, E. Palomares, J. Ko, M. Grätzel, T. Torres, Angew. Chem. Int. Ed. 46 (2007) 8358.
[16] J.-M. Chrétien, A. Mallinger, F. Zammattio, E. Le Grognec, M. Paris, G. Montavonc, J.-P. Quintarda, Tetrahedron Lett. 48 (2007) 1781.
[17] (a) G.R. Robertson, Org. Synth. Coll. 1 (1941) 396;
(b) G.R. Robertson, Org. Synth. Coll. 2 (1922) 57.
[18] J.K. Laha, S. Dhanalekshmi, M. Taniguchi, A. Ambroise, J.S. Lindsey, Org. Process. Res. Dev. 7 (2003) 799.
[19] C.Y. Lin, Y.C. Wang, S.J. Hsu, C.F. Lo, E.W.G. Diau, J. Phys. Chem. C 114 (2010) 687.
[20] C.F. Lo, L. Luo, E.W.G. Diau, I.J. Chang, C.Y. Lin, Chem. Commun. (2006) 1430.
[21] Q.J. Sun, H.Q. Wang, C.H. Yang, Y.F. Li, J. Mater. Chem. 13 (2003) 1377.
[22] (a) Z.J. Ning, Q. Zhang, W.J. Wu, H.C. Pei, B. Liu, H. Tian, J. Org. Chem. 73 (2008) 3791;
(b) R.Z. Li, D. Shi, D.F. Zhou, Y.M. Cheng, G.L. Zhang, P. Wang, J. Phys. Chem. C 113 (2009) 7469.
[23] Z.S. Wang, Y. Cui, Y. Dan-oh, C. Kasada, A. Shinpo, K. Hara, J. Phys. Chem. C 111 (2007) 7224.
[24] N.R. Neale, N. Kopidakis, J. van de Lanemaat, M. Grätzel, A.J. Frank, J. Phys. Chem. B 109 (2005) 23183.
[25] A.C. Khazraji, S. Hotchandani, S. Das, P.V. Kamat, J. Phys. Chem. B 103 (1999) 4693.
[26] (a) F. Fabregat-Santiago, J. Bisquert, L. Cevey, P. Chen, M. Wang, S.M. Zakeeruddin, M. Grätzel, J. Am. Chem. Soc. 131 (2009) 558;
(b) M. Adachi, M. Sakamoto, J. Jiu, Y. Isoda, J. Phys. Chem. B 110 (2006) 13872.
[27] Q. Wang, J.E. Moser, M. Grätzel, J. Phys. Chem. B 109 (2005) 14945.
[28] Q. Wang, S. Ito, M. Grätzel, F. Fabregat-Santiago, I. Mora-Sero, J. Bisquert, T. Bessho, H. Imai, J. Phys. Chem. B 110 (2006) 25210.
[29] (a) R. Kern, R. Sastrawan, J. Ferber, R. Stangl, J. Luther, Electrochim. Acta 47 (2002) 4213;
(b) C. Longo, A.F. Nogueira, M.A. Paoli, H. Cachet, J. Phys. Chem. B 106 (2002) 5925.
[30] J. Van de Lagemaat, N.G. Park, A.J. Frank, J. Phys. Chem. B 104 (2000) 2044.
[31] H.C. Choi, S. Kim, S.O. Kang, J. Ko, M.S. Kang, J.N. Clifford, A. Forneli, E. Palomares, M.K. Nazeeruddin, M. Grätzel, Angew. Chem. Int. Ed. 47 (2008) 8259.